JAEA-Research
2008-051

JAEA-Research

Parameter Dependence on the Lower Hybrid Driven Current in Tokamaks

Kazuya UEHARA and Takashi NAGASHIMA*

Tokamak Experimental Group
Fusion Research and Development Directorate

March 2008

Japan Atomic Energy Agency

日本原子力研究開発機構

本レポートは独立行政法人日本原子力研究開発機構が不定期に発行する成果報告書です。
本レポートの入手並びに著作権利用に関するお問い合わせは、下記あてにお問い合わせ下さい。
なお、本レポートの全文は日本原子力研究開発機構ホームページ（http://www.jaea.go.jp）
より発信されています。

独立行政法人日本原子力研究開発機構　研究技術情報部　研究技術情報課
〒319-1195　茨城県那珂郡東海村白方白根 2 番地 4
電話 029-282-6387, Fax 029-282-5920, E-mail:ird-support@jaea.go.jp

This report is issued irregularly by Japan Atomic Energy Agency
Inquiries about availability and/or copyright of this report should be addressed to
Intellectual Resources Section, Intellectual Resources Department,
Japan Atomic Energy Agency
2-4 Shirakata Shirane, Tokai-mura, Naka-gun, Ibaraki-ken 319-1195 Japan
Tel +81-29-282-6387, Fax +81-29-282-5920, E-mail:ird-support@jaea.go.jp

Parameter Dependence on the Lower Hybrid Driven Current in Tokamaks

Kazuya UEHARA and Takashi NAGASHIMA*

Division of Advanced Plasma Research
Fusion Research and Development Directorate
Japan Atomic Energy Agency
Naka-shi, Ibaraki-ken

(Received, March 4, 2008)

Summary - An optimum efficiency and the current profile on the lower-hybrid driven current in tokamaks are estimated in a semi-empirical model by the modified quasi-linear theory, in which the effect of the mode conversion, the accessibility condition and the non-linear effect of the parametric instability as well as the artificial term of the parallel reflective index for the spectrum gap are introduced so as to coincide with experimental data. It is shown that an optimum parallel reflective index for the substantial current flowing must be less smaller for the higher electron temperature plasma not to disturb the accessibility condition and that the driving efficiency depends on the electron temperature as well as the plasma density, in which the latter leads that the higher operating frequency can enable an effective current flowing for the higher density plasma. The surveying parameters are used in the JT-60 lower-hybrid current drive (LHCD) experiment and the estimation is also performed for the parameter of the next generation machine ITER.

Keyword: Lower-hybrid Current Drive, Modified Quasi-linear Theory, Spectrum Gap, N Parallel, Gap Parameter, Current Profile

---

Nippon Advanced Technology Co., Ltd

トカマクにおける低域混成波による電流駆動のパラメーター依存

日本原子力研究開発機構
核融合研究開発部門　先進プラズマ研究開発ユニット
上原　和也、永島　孝*

（２００８年３月４日受理）

トカマクにおける低域混成波による電流駆動の最適な駆動効率と径方向の電流分布を、色々なガウス型の n_z スペクトル($= \exp(-(n_z-n_{zc})^2/h_z)$)に対して、修正された準線形理論と簡単な rf 減衰モデルを用いて経験的に評価した。修正された準線形理論は実験的に得られている駆動電流が説明できるように、モード変換と近接性及びパラメトリック不安定性によるパワー吸収離脱を考慮したものである。さらに、実験と合うように駆動効率を新たに定義し、パワー密度に依存するギャップパラメーターをスペクトルギャップを埋める為に導入している。最適な進行波による低域混成波の屈折率の n_z スペクトルの中心値 n_{zc} は電子温度が高い時は近接性を乱さない程度の小さな値であり、最適な駆動効率はプラズマの電子温度に依存し、密度が高い領域では印加可周波数が高いことが要請される。計算は JT-60 のパラメーターと次期装置の ITER のパラメーターに対してなされた。

那珂核融合研究所（駐在）：〒311-0193　茨城県那珂市向山 801-1
*日本アドバンス・テクノロジーOB

Contents

目次

This is a blank page.

1. INTRODUCTION

Although the great progress in experiments[1] on the lower hybrid current drive (LHCD) for aiming the stationary operation of the fusion reactor, the modeling of this phenomena has been so complicated and the evaluated results does not reach the final goal of satisfactory understanding. The modeling is usually carried out by combining a ray tracing (RT) code to a solution of the Fokker-Planck (FP) equation including the quasi-linear scheme[2] and reproduces at least qualitatively some of the experimental trends, although inconsistencies are still remained[3]. First, the density limit exists experimentally, that is, the substantial flowing current of the LHCD could not be obtained for the more than a certain critical density, which cannot be predicted by the RT/FP modeling although it can be explained that the driving efficiency is inverse proportional to the density as is predicted experimentally. Second, the used parallel reflective index $N_{//}$ in experiments is too small to couple thermal electrons effectively in resultant to cause so small current, which is the so-called the spectrum gap problem to be the long-lasting debate in the LHCD modeling. Third, the calculated current profile is so off-axis to cause so small current flowing compared with the experiment. For the first item, we have already showed that the density limit must be deduced to the complete deprivation of the rf power in plasma due to non-accessibility, mode conversion and the parametric instability in resultant the deformation of the electron distribution function may be disappeared[4]. For the second item, although many calculations using the RT/FP are reported[5, 6] these calculations cannot predict experimental results reasonably, in which it is not enough in the up-shift of $N_{//}$ and more further up-shift is necessary that can form the substantial current of the LHCD observed in the experiment[7]. For the third item, it is one of reasons that the regular application of the LHCD attempt to a core plasma current formation in the next generation tokamak (ITER) is hesitated.

In this paper, we want to report a significant calculated results in which we remind that above discrepancies must be avoided and that we must reflect the experimental results, although we use the simple slab model in the lower-hybrid wave propagation. In addition to the quasi-linear theory, we introduce three criteria to determine the deprivation of the rf power in plasma, that is, the accessibility condition, the mode conversion and the parametric instability are considered in the calculation of the rf power propagation in the plasma for solving above first discrepancy. The problem of the spectrum gap is related to the electron temperature as shown in Fig. 1, in which the relation of the value of ω against the rf power density ρ in the LHCD experiment in the world, where ω is the phase velocity v_z normalized by the electron thermal velocity v_{the}, $\omega=v_z/v_{the}$, and we estimate this value from $N_{//}$ and the average electron temperature in each machine, where $v_z=c/N_{//}$ and c is the velocity of light. The quasi-linear prediction says that the optimum ω for the substantial current flowing in the LHCD is to be $\omega=2.5\sim4$ which is shown by shadow region, whereas the real ω is

always larger than this value in all machine to be more than five times larger in maximum. It should be noted that this value increases with decrease of ρ and decreases with increase of ρ, whose survey is evaporated as $\omega=13.2\rho^{-0.28}$ as shown in Fig.1. So, we introduce the gap parameter being inverse proportional to the value of ρ to bury the spectrum gap between the experimental rf spectrum and the real one. In section 2, the formation of calculation is shown. Parameter dependence of the driving efficiency is shown in section 3. Discussions and summary are shown in section 4.

2. FORMATION OF CALCULATION

The direct way to estimate the plasma current I_{rf} is to calculate the following value.

$$I_{rf} = \int_0^a j_{rf} 2\pi r dr \tag{1}$$

, where a is the plasma minor radius and j_{rf} is given

$$j_{rf} = env_{the} \int_{-\infty}^{\infty} \omega \exp\left(\int^{\omega} \frac{-\omega}{1+\omega^2 D_{ql}}\right) d\omega d\omega \tag{2}$$

where, D_{ql} in the inner integral is zero when $\omega < \omega_1$ and $\omega > \omega_2$ and is not zero otherwise to be expressed as

$$D_{ql} = \frac{\pi e^2}{m_e^2} \frac{E_{rf}^2}{v_z \Delta k_z \nu_0 v_{the}^2} \tag{3}$$

where e is electron charge, m_e is mass of electrons, E_{rf} is the rf electric field in plasma, Δk_z is half width of the wave number, $\nu_0(=4\pi(Z_{eff}+2)n_e e^4 \ln\Lambda/m_e^2 v_{the}^3)$ is collisional frequency and ω_1, ω_2 are the lower and upper limit of the injected rf spectrum[8]. Here, we apply a slab model in the calculation of E_{rf} as the zeroth order approximation, that is, the variation of D_{ql} is calculated through P_{rf} as $dP_{rf}/dr = -2k_{ql}P_{rf}$, where k_{ql} is the quasi-linear spatial damping rate[8]

$$k_{ql} = \sqrt{\frac{\pi}{8}} \frac{\omega^3}{1+2\omega^3 D_{ql}} e^{-\omega^2 \frac{(k_x^2+k_z^2)^2}{k_x k_z^2}} \tag{4}$$

, where k_x is the perpendicular wave number and E_{rf} is calculated to connect P_{rf} using resonance cone model[9)]

$$E_{ql} = \sqrt{\frac{8\pi}{P_{rf}}} \frac{1}{\sqrt{1+k_x^2/k_z^2}\sqrt{1+\omega_{pe}^2/\omega_{ce}^2}} \sqrt{\frac{a}{Sr v_g}} \tag{5}$$

, where ω_{pe} $(=(e^2 n_e/\varepsilon_0 m_e)^{1/2})$ and $\omega_{ce}(=eB/m_e)$ are electron plasma and cyclotron frequency, S is the area of wave guide, $B=(B_t^2+B_p^2)^{0.5}$, v_g is the group velocity of the lower hybrid wave, B_t is toroidal magnetic field and B_p is poloidal magnetic field[9)].

$$v_g = \frac{c}{n_{zc}} \frac{(\omega^2/\omega_{LH}^2 - 1)^{3/2}}{\omega^2/\omega_{LH}^2} \frac{\omega_{pe}^2}{\omega_{ce}^2} \tag{6}$$

, where $\omega(=2\pi f)$ is the injected rf wave, ω_{LH} $(=\omega_{pi}/(1+\omega_{pe}^2/\omega_{ce}^2)^{1/2})$ is the lower hybrid frequency, $\bar{n}_{zc}$ is the average value of $N_{//}$. The rf power spectrum P_{rf} is Gaussian, which is

$$P'_{rf} = \frac{P_{rf0}}{\sqrt{h_z}} \exp\left(-\frac{(n_z - n_{zc})^2}{h_z}\right) \tag{7}$$

, where $N_{//}$ is denoted by n_z and n_{zc} from here and this value connects to the value of P_{rf} in eq.(5) as

$$P_{rf} = y_M y_P \int_{n_{za}}^{\infty} P'_{rf} d n_z \tag{8}$$

where n_{za} is the lower n_{zc} to satisfy the accessibility condition as,

$$n_{za} = \frac{\omega_{pe}}{\omega_{ce}} + \left(1 + \frac{\omega_{pe}^2}{\omega_{ce}^2} - \frac{\omega_{pe}^2 \omega_{ci}}{\omega_{ce}\omega_0^2}\right)^{1/2} \tag{9}$$

which is the first constraint of the rf power, where $\omega_{pi}(=Z_{eff}eB/m_i)$ is the ion plasma frequency, Z_{eff} is the effective charge state and m_i is the mass of ions. Setting $\omega_1=v_{z1}k_1$, $\omega_2=v_{z2}k_2$, $\Delta k=k_2-k_1$, $v_{z1}=c/N_1=c/n_{z1}$ and $v_{z2}=c/N_2=c/n_{z2}$ then Δk_z in eq.(4) is expressed $\Delta k_z=\Delta k=\omega_2 n_{z2}/c-\omega_1 n_{z1}/c$, $n_{z2}=n_{zc}+(4h_z \ln 2)^{0.5}$, $n_{z1}=n_{zc}-(4h_z \ln 2)^{0.5}$. Second constraint is the mode conversion condition. The value of y_M in eq.(8) is $y_M=0$ for $\omega/\omega_{LH}<1$, $y_M=((\omega/\omega_{LH})^2-1)$ for $1<\omega/\omega_{LH}<2$ and $y_M=1$ for $\omega/\omega_{LH}>2$, Third constraint

is on the parametric instability. The value of y_P in eq.(8) is $y_P=1$ for $\gamma < \gamma_{c1}$ and $y_P=0.53\gamma^2-2.53\gamma+3$ for $\gamma_{c1} < \gamma < \gamma_{c2}$ and $y_P=0$ for $\gamma > \gamma_{c2}$, where γ is growth rate of the parametric instability which is $\gamma=2.67 \times 10^{-11} T_{es}^{-1.55} n_e^{2.08} B_t^{-3.45}$, where $T_{es}=T_{e0}[1-(r/1.08a)^2]^2$, $n_e=n_{e0}[1-(r/1.08a)^2]^2$, $B_t=B_{t0}R/(R+r)$, T_{e0} in eV, n_e in cm^{-3} and B_t in Gauss. These are experimentally obtained in JFT-2[10]. These constraints on P_{rf} are shown graphically in Fig. 2. Thus, in this paper it is considered that the density limit in the LHCD occurs when D_{ql} in eq.(2) becomes zero through P_{rf}.

Usual toroidal effect is considered as $n_{zc}'=n_{zc0}(R+a)/(R+r)$, where n_{zc0} is the value of n_z at r=a. As shown in Fig. 1, it is known experimentally that the gap is smaller when ρ is larger and/or T_e is higher, which is in the case of JT-60[11] and Alcator-C[12, 13] and that/or the gap is larger when ρ is smaller and T_e is lower, which is in the case of WT-II[14] and PLT[15]. In addition to above toroidal effect the rf spectrum must be further up-shifted by the gap parameter G_{sp} as $n_{zc}''=G_{sp}n_{zc0}$, where n_{zc0} is n_{zc} without gap parameter, that is, $G_{sp}=b/\rho^{\alpha}$, where ρ is in kW/cm^2. Including these constraints we can get a plausible calculation that can bear the experimental results. In another word, we can determine the numerical factor of b and α to fit the experiments. The driving efficiency is defined using eqs.(1) – (9) as

$$\eta_{CD} = \frac{\bar{n}_e I_{rf} R}{P_{rf0}} \tag{10}$$

where $\bar{n}_e$ is average plasma density. It should be noted that we do not use the value of p_d as

$$p_d = \int_{-\infty}^{\infty} dv_z \frac{1}{2} m v_z^2 \frac{\partial}{\partial v_z} D_{ql} \frac{\partial f}{\partial v_z} \tag{11}$$

for η_{CD} because this value is the deposited power into the plasma[2], which cannot be measured directly.

3 PARAMETER DEPENDENCE

(1) Flowing current and optimum driving efficiency

The evaluated density dependence of I_{rf} for the PETULA-B parameters (T_{e0}=830 eV, P_{rf}=1 MW and n_{zc}=2.3) are calculated against $\bar{n}_e$ as shown in Fig.3, where this machine was a medium sized former tokamak in France. We can see that I_{rf} with decreases of $\bar{n}_e$ and decreases drastically beyond the certain density. If we consider the quasi-linear effect only I_{rf} is solely decreasing with increasing $\bar{n}_e$ as shown by the

dotted line in this figure, where γ_{c1} and γ_{c2} are determined from the experimental data observed by the electrostatic probe in JFT-2[10]. These are well corresponds to the experimental result in PETULA-B[16].

The evaluated flowing current I_{rf} as well as η_{CD} are calculated against the value of n_{zc} for the JT-60 parameters ($\bar{n}_e$= 3 x 10^{12} cm^{-3}, B_{t0}= 4 T, f= 2GHz and P_{rf}= 1 MW) as shown in Fig.4, where this machine was the former tokamak of the JT-60U and we can see that I_{rf} as well as η_{CD} increases with increase of T_{e0} and there exists an optimum n_{zc} for the lager η_{CD} and that the smaller n_{zc} is better for the larger electron temperature as long as the accessibility is not destroyed. The effect of the accessibility is seen in this calculation, where the efficient profile of I_{rf} is asymmetric on n_{zc} around the peaked value of I_{rf} at the optimum n_{zc}. This is because the rf power is effectively absorbed with the high accessibility condition and the profile of I_{rf} becomes more sharp on n_{zc} for higher density case ($\bar{n}_e$= 1 x 10^{13} cm^{-3}, T_{e0}= 3keV) as shown by the dotted curve in Fig. 4.

Figure 5 shows I_{rf} and η_{CD} against the central electron temperature T_{e0} for the same parameter of Fig. 4 putting n_{zc} as a parameter. Recent experimental results on JT-60 indicates that the driving efficiency increases with the electron temperature[17].

Density dependence of I_{rf} is calculated in Fig. 6 for JT-60 and ITER parameters[18], where the frequency is 2 GHz for JT-60 and 4 GHz, 8 GHz for ITER case with various of T_{e0} and ρ as shown in the top corner of Fig. 6. In the ITER case the operating gas is deuterium (D_2). It is known that there exists the optimum density for flowing the current of the LHCD as shown by allows in Fig. 6. It should be noted that empirical scaling on $I_{rf} \propto 1/\bar{n}_e$ is only valid when the density is smaller at a critical density as shown by opened allows in Fig. 6. When the density is too small the rf current increase with decreasing $\bar{n}_e$ which is already seen at $\bar{n}_e$ < 2 x 10^{12} cm^{-3} in PETULA-B case as shown in Fig. 3. This may be coming from the density dependence of the group velocity v_g in eq.(6). Beyond the critical density the deposited rf power to electrons is reduced drastically by the power derivation due to the mode conversion, the non-accessibility and the parametric instability for the flowing current to drop rapidly, which is what we call the density limit. The higher operation frequency can enable to improve the possible density region for the current drive and can enlarge the density limit, which cannot be driven by only the quasi-linear theory. Possible density region of the current drive is also affected by the rf power density, which are seen in the ITER case of 2 kW/cm^2 and 4 kW/cm^2 in Fig. 6.

(2) Current profile

The current profile in JT-60 and ITER parameters are calculated putting n_{zc} and T_{e0} as parameters as shown in Figs. 7, 8 and 9. In JT-60 case, the current is peaking at n_{zc}=1.2 and is hollow at n_{zc}=2.2 as shown in Fig.7, which is well correspond the experiment[19]as discussed in the next section. The current profile in ITER is not so

hollow if we chose the small n_{zc}(n_{zc}<1.15 at 20 keV) and not so larger electron temperature (T_e < 20 keV at n_{zc} = 1.0) as shown in Figs. 8 and 9. The problem is in the accessibility condition whether we can realize the up-shift of n_{zc} by raising the magnetic field and the operating frequency any more. It is expected that the hollow current profile in the lower-hybrid current drive must be further buried by the radial diffusion that is omitted in the Fokker-Planck equation[20] and the pinch effect due to the resonant electrons[21].

4 DISCUSSIONS AND SUMMARY

The LHCD calculation must be evaluated taking into account consistently the effect of the quasi-linear interaction in the wave propagation and collisions as well, in which the toroidicity and the deposition of the main power spectrum must be properly considered[22]. The power deprivation of the rf wave during the wave propagation due to the parametric instability, the accessibility condition and the prohibition condition of the mode conversion is adequate to predict the density limit of PETLA parameter as shown in Fig. 3 and that of JT-60 and ITER case are predicted as shown in Fig. 4, however, it must be further checked whether the validity to use the growth rate of the parametric instability observed in JFT-2 would be available for other machines. It is further shown that the density limit can be enlarged if we can get higher electron temperature to suppress the parametric instability, the higher magnetic field to avoid the non-accessibility and the raising the injected frequency to avoid the mode conversion. We do not have so clear physical validity of the type of function on y_M and y_P, where these term are introduced so that the calculation make to correspond to experiments in quality and in quantity.

To the gap parameter introduced in this paper must be given a probable physical meaning. It is reported that the use of multi-path technique may give appropriate up-shift of $N_{//}$[23], however, the choice of the path seem to be rather arbitrary, which cannot be easily found the probable physical reason. In general, when the strong damping occurs at the higher electron temperature with large spectrum gap that the rf power is absorbed by single path the RT/FP model can predict the LHCD experimental results and the problem in the RT/FP model is when the weak damping occurs at the lower electron temperature with small spectrum gap that the rf power is absorbed by multi path. The scaling of $\omega=13.3\rho^{-0.28}$ in Fig. 1 includes the dependence of the electron temperature through v_{the} and the higher ρ corresponds to the high electron temperature case, which is well reflecting to the problem of FT/FP model, that is, when the larger ρ case corresponds to the higher electron temperature case, which is small spectrum gap and the smaller ρ case is lower electron temperature case, which is large spectrum gap. It should be noted that the calculated current in JT-60 case using ray tracing show almost zero by the single ray having too small up-shift of $N_{//}$[24].

It should be noted that if we use eq.(11) the efficiency has no dependence on T_e as

long as T_e is not so high, whereas if we use eq.(10) the efficiency has a dependence on T_e even for the lower T_e. In the case using p_d, it is quite deserved for the efficiency to have no dependence on T_e since j_{rf} and p_d has a similar dependence on T_e in resultant to cancel out by dividing j_{rf} by p_d. This is considered because the extent of the absorption to resonant electrons is changed during the wave propagation in plasma which may be a function on T_e. The larger T_e may cause the increment of resonant electrons and the decrement of collisions in resultant to increase the current although wave damping becomes larger with increase of T_e. The larger electron temperature and the larger rf power are better for the large current at the optimized n_{zc}. The latter can lead that the efficiency is better for the sharp rf spectrum, which is already confirmed experimentally[25]. And this is important item which is obtained in this paper. The value of p_d in eq.(10) is the power to be absorbed by plasmas to hold the deformation of electron distribution function f.

In JT-60 the higher driving efficiency of 3.4 x 10^{19} $AW^{-1}m^{-2}$ is already obtained experimentally, which is almost close to the ITER calculation on the LHCD(=3 ~ 4 x $10^{19}AW^{-1}m^{-2}$) for T_e= 20 keV. However, it is difficult to consider that these experimental value in JT-60 may keep almost same value for the larger electron temperature of 20 keV. It is afraid that the conventional calculation in the LHCD may be almost one order smaller than the real situation, because that the experimental efficiency is proportional to T_e is one of reasons. It is estimated that the experimental efficiency of 3.4 x 10^{19} $AW^{-1}m^{-2}$ can be evaporated to the larger value of 3.2 x $10^{20}AW^{-1}m^{-2}$ at T_e= 20 keV if we assume for the efficiency to be proportional to T_e. However, the efficiency must saturate and/or decrease with increase of T_e as long as we does not choose the less $N_{//}$ for large T_e as shown in Fig.5. If we set the optimum n_{zc} to be n_{zcc} as indicated by arrows in Fig.4, the driving efficiency is evaporated as $\eta_{CD}=0.1<T_e>^{0.1/nzcc}$ x 10^{20} $AW^{-1}m^{-2}$, which is about one order larger than NBI current drive efficiency[26, 27], in which the experimentally observed current drive efficiency η_{CD} against the electron temperature in various machines for LHCD, NBCD and ECCD are shown in Fig. 10. It should be better to use the LHCD in ITER rather use the NBCD as well as ECCD since the efficiency is quite lower in the latter.

The dependence of I_{rf} is quite natural to be evaluated as shown in Fig. 4 and Fig. 7 of JT-60 case, where the spatial distribution as well as the intensity of the hard X ray signal are shown in Fig. 10[19] although the signal of hard X ray does not directly reflect the current induced by the LHCD. We equipped four channel X ray diagnostics in the radial direction as shown in Fig. 10 (a). The dependence on $N_{//}$ of these signals are shown in Fig. 10 (b), in which we can see that the optimum $N_{//}$ has a peak value at about 1.4 as indicated in the calculation of Fig. 4. The Abel transformed radial profile using emission signals measured at r/a=0.23(ch1), r/a=0.57 (ch2.) and r/a=0.86 (ch.3) are shown in Fig. 10 (c), in which we can see that relatively small number of high energy electrons are localized at the center with smaller $N_{//}$ and small number of the tails are in the outer with larger $N_{//}$ as indicated in the calculation of Fig. 7. Similar

modeling and the calculation of high energy electron tails in the LHCD experiment is also performed in PLT[28]. The spectrum gap problem discussed here is recently reported in connection with the parametric decay instabilities[29].

In summary, we can get the following statements.

(1) Simple slab model calculation adding the condition of power deprivation due to mode conversion and parametric instability introducing gap parameter in addition to the quasi-linear theory can give plausible explanation of the lower-hybrid current drive experiment.

(2) The optimum $N_{//}$ exists for the optimum driving efficiency which lead the sharp spectrum is better and the smaller $N_{//}$ is necessary for higher electron temperature plasma not to destroy the accessibility.

(3) Optimum driving efficiency increases with the electron temperature at lower temperature and saturate or decrease unless the smaller $N_{//}$ does not use.

(4) Driving current increases with the density till a certain density and decreases with $\bar{n}_e$ till the rf power is lost completely by the parametric decay wave, accessibility and the mode conversion, where the critical density enlarged by raising the operating frequency.

Finally, it is stressed that this calculation presented here does not include the power deposition due to α particle and that the quasi-linear theory is assumed to be valid to apply such current drive experiment.

Acknowledgements

Technical performance of the simulation by Dr. R. Imanishi in Fujitsu FIP cooperation is appreciated. Discussions with Dr. T. Yamamoto and Dr. M. Hatayama in Toshiba cooperation (now in Keio University) are appreciated.

References

1) T. Yamamoto et al., Phys. Rev. Lett, **45**, 716 (1980)
2) N. Fisch, Phys. Rev. Lett, **41**, 873 (1978)
3) W. A. Houlberg et al., Nucl. Fusion 45 (2005) 1309
4) K. Uehara et al., Nucl. Fusion **29**, 753 (1988)
5) P.T. Bonoli et al., Nucl Fusion **28**, 99(1988)
6) D.L. Grekov et al., Sov. J. Plasma Phys. **10**, 654 (1984)
7) K. Kupfer et al., Phys. Fluids **B 5**, 4391 (1993)
8) S. Yuen, D. Kaplan and D.R. Cohn, Nucl. Fusion **20** 195 (1980)
9) T. Yamamoto, T. Imai, M. Shimada, H. Takeuchi et al., J. Phys. Soc. Jpn, **48**, 1349 (1980)
10) K. Uehara, H. Takeuchi et al., J. Phys. Soc. Jpn. **49** 2364 (1980)
11) Y. Ikeda et al., Nucl. Fusion **29**, 1815 (1989)

12) M. Porkolab, IEEE, Trans. Plasma Sci. **PS-12**, 107 (1984)
13) M. Porkolab et al., Phys. Rev. Lett. **53**, 450 (1984)
14) S. Kubo, M. Nakamura et al., Phys. Rev. Lett. **50**, 1994 (1983)
15) S. Bernabei, C. Daughney et al., Phys. Rev. Lett. **49**, 1255 (1982)
16) G. Gormezano , G. Agariti et al. Proc. 10th IAEA 1984 F-II-5 Nucl Fusion Suppl p.503
17) K. Ushikusa et al., Nucl . Fusion **29**, 1052 (1989)
18) ITER documenmt series No. 32 1991
19) K. Uehara et al., AIP Conf. proceeding 190, Radio-frequency power in plasmas, 8th Topical Confernce , Irvine CA 189, p.106
20) J.M. Rax and D. Moreau, Nucl Fusion **29**, 1751 (1989)
21) K. Uehara J. Phys. Soc. Jpn, **53**, 2018 (1984)
22) R. Cesario et al., Nucl. Fusion. **46**, 462 (2004)
23) F. Imbeax and Y. Peysson, Plasma Phys. Control. Fusion **47**, 2041 (2005)
24) K. Ushigusa et al., JAERI-M 89-033
25) J. Stevens et al., Nucl. Fusion **28**, 217 (1988)
26) J. G. Cordey et al., Plasma Phys. **24**, 73 (1982)
27) R. David, Nucl. Technology **4**, 237 (1983)
28) J. Stevens et al., Nucl. Fusion **25** , 1529 (1985)
29) R. Cesario et al., Phys. Rev. Lett. **92**, 15700-1 (2004)

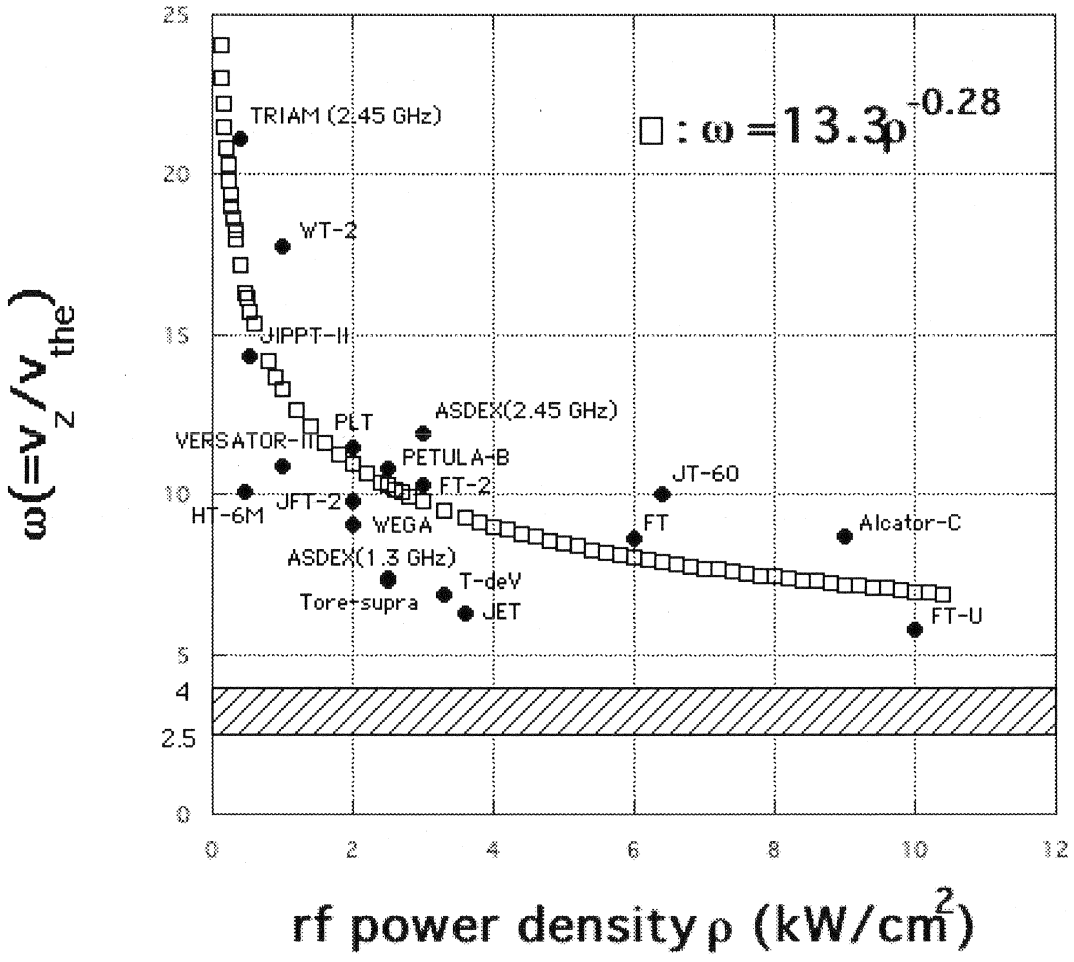

Fig. 1 Summary of the spectrum gap in the LHCD machines in the world, where the normalized phase velocity($\omega=v_z/v_{the}$) is shown against the power density ρ(kW/cm^2) . Experimental data can fit the curve of $\omega=13.3\rho^{-0.28}$ and the optimum ω predicted by the theory is expressed by shadow.

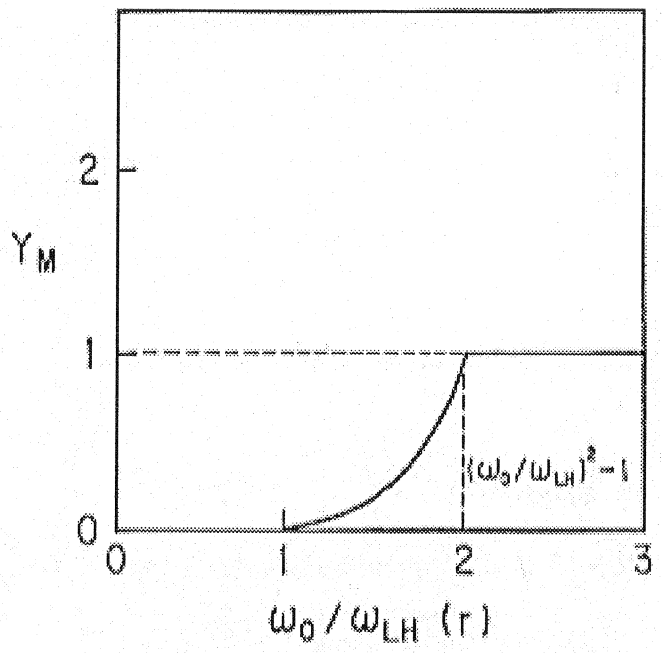

(a)

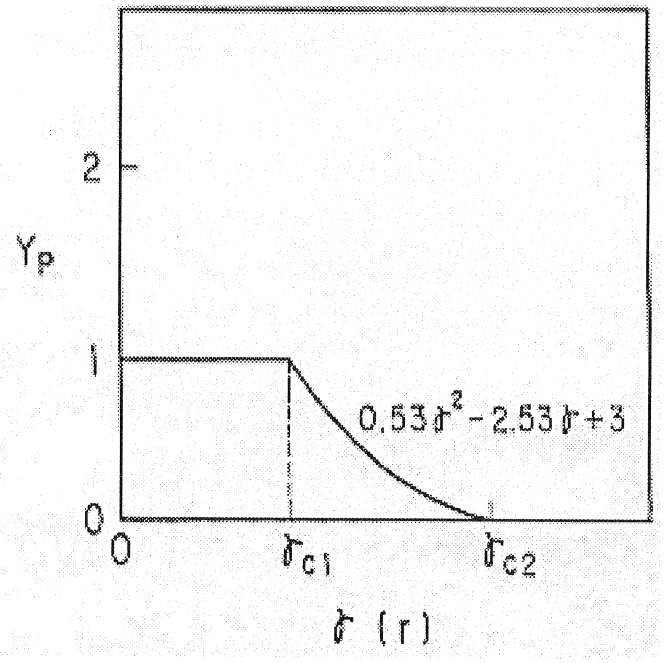

(b)

Fig. 2 The value of y_M and y_p in eq.(8) are graphically shown against $\omega_0/\omega_{LH}(r)$ and the growth rate γ (r)in (a) and (b), respectively, which becomes the constraint for the rf power P_{rf} in the performance of the simulation.

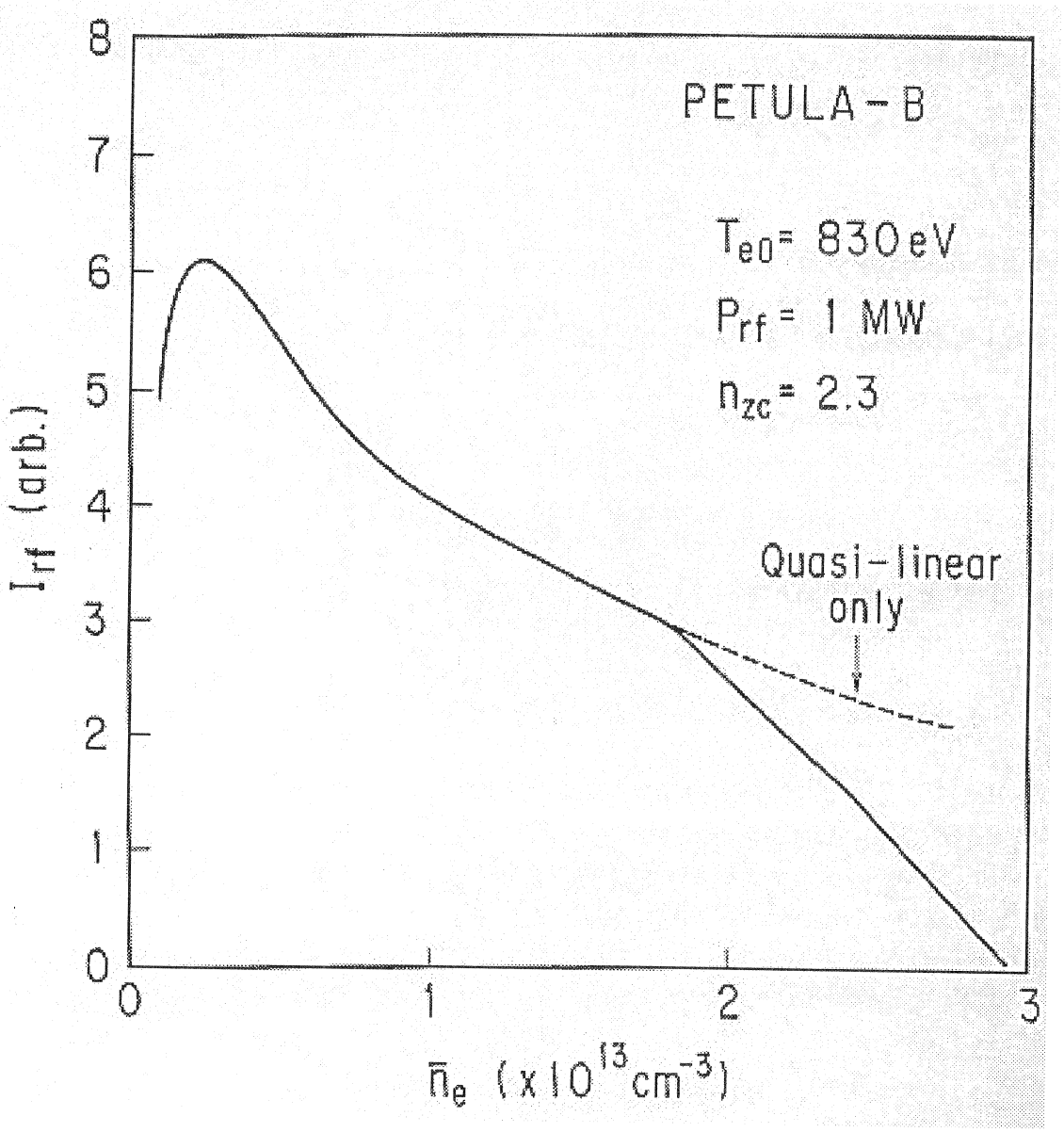

Fig. 3 Evaluated rf current I_{rf} of the LHCD against $\bar{n}_e$ for PETRLA-B parameters, where b=21.9, α=0.23, γ_{c1}=1, γ_{c2}=4.24 and ρ= 2.5 kW/cm^2. Dotted curve is obtained when Y_M=1 and Y_p=1.

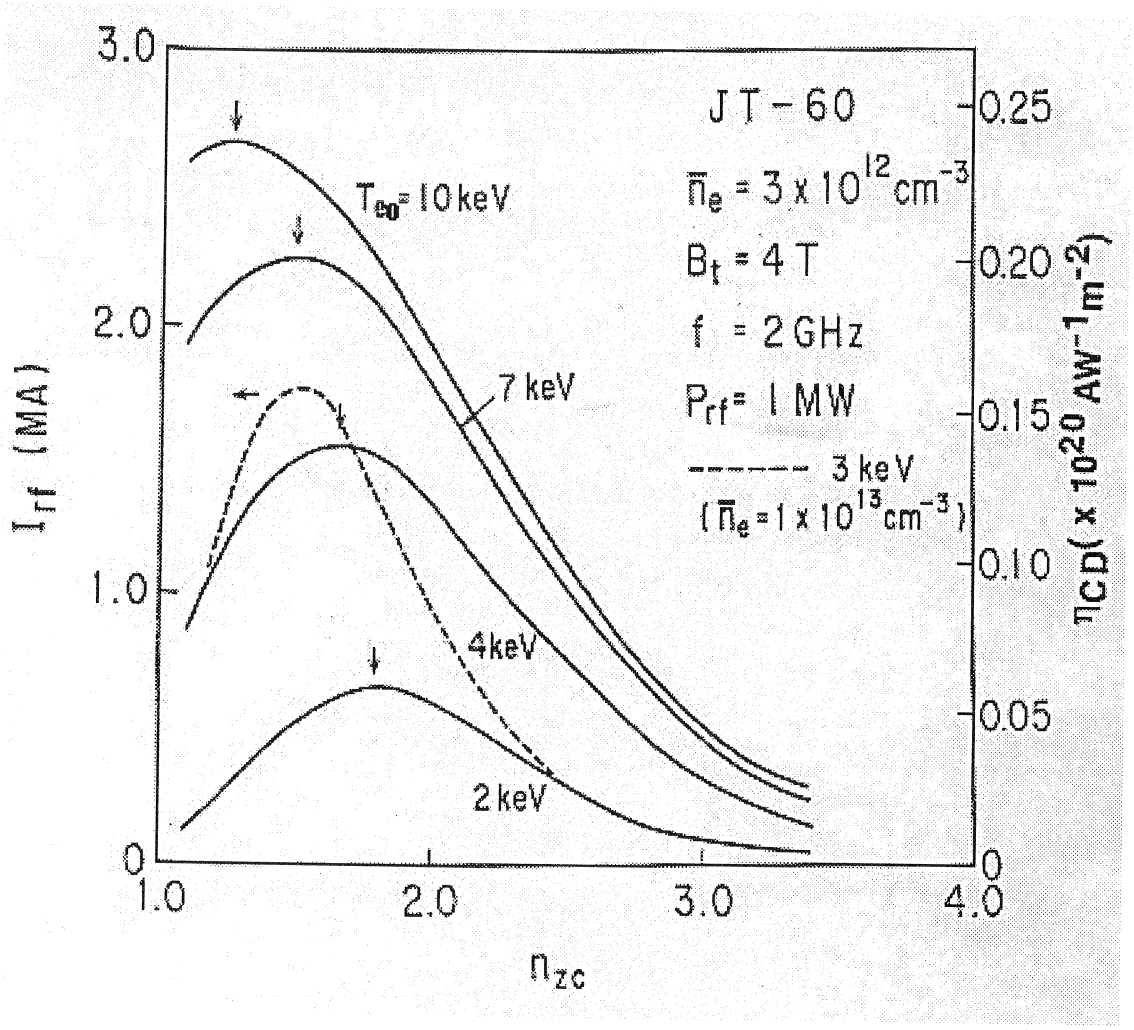

Fig. 4 Evaluated I_{rf} and η_{CD} vs n_{zc} putting T_{e0} as parameters in JT-60 case, where b=21.9, α=0.23, $\gamma_{\chi 1}$=1, γ_{c2}=4.24 and ρ= 4 kW/cm^2. Dotted curve is for T_{e0}= 3 keV and $\bar{n}_e$=1 x10^{13} cm^{-3} case.

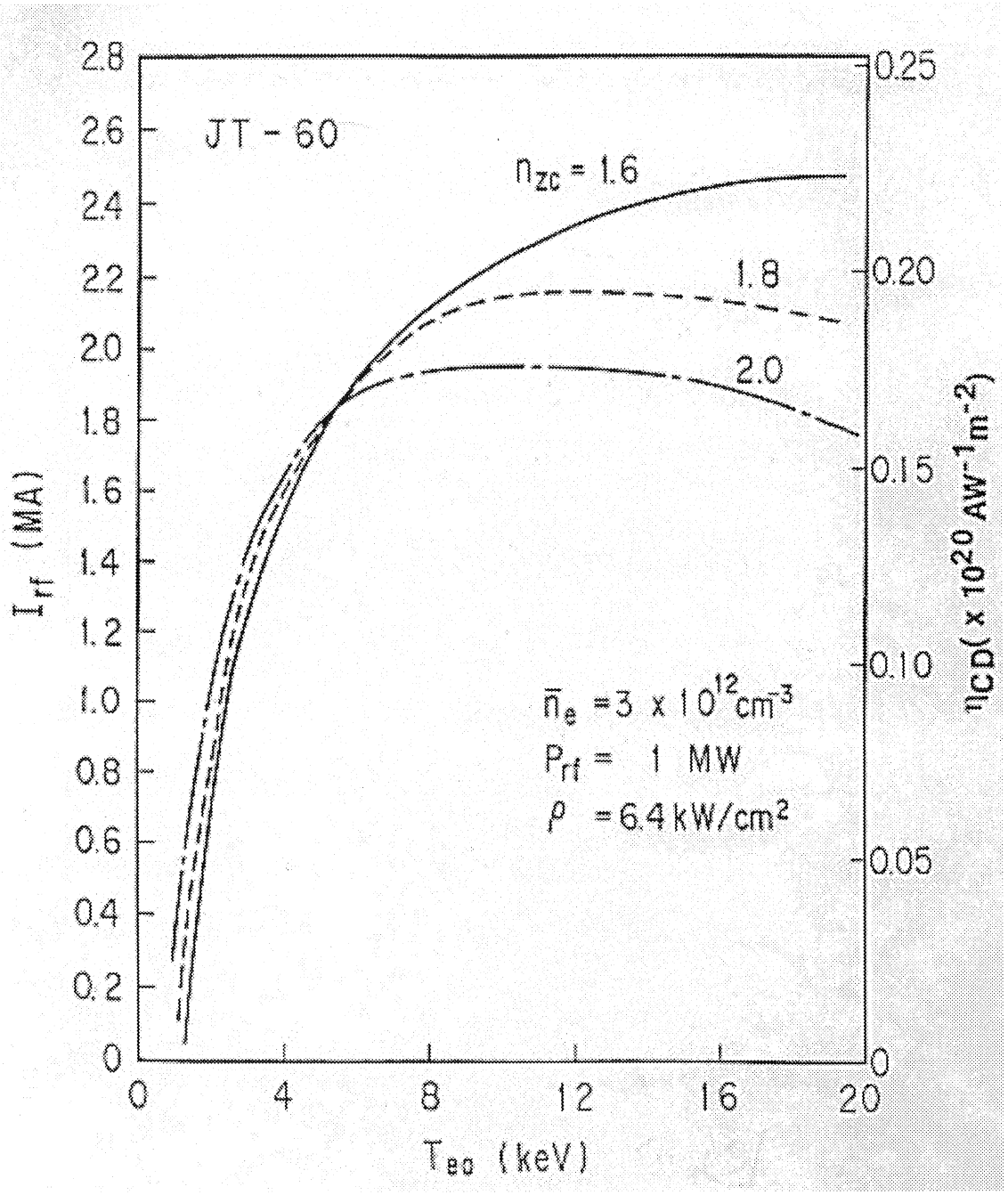

Fig. 5 Evaluated I_{rf} and η_{CD} vs n_{zc} putting P_{rf} as parameters in JT-60 case, where b=21.9, α=0.23, $\gamma_{\chi l}$=1, γ_{c2}=4.24 and ρ= 6.4 kW/cm^2.

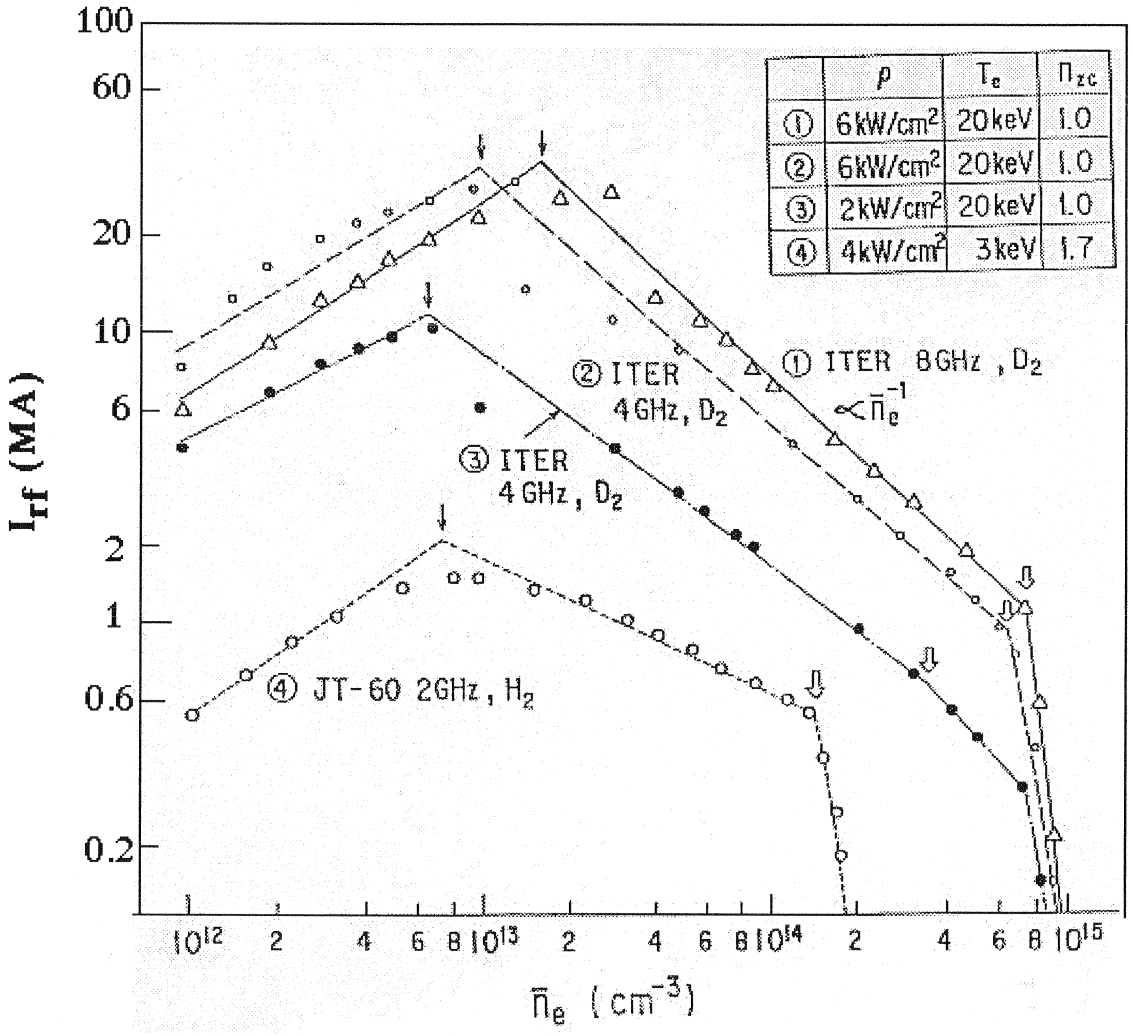

Fig. 6 Evaluated density dependence of I_{rf} in JT-60 and ITER case, where b=21.9, α=0.23, $\gamma_{\chi 1}$=1, γ_{c2}=4.42 and using parameter of ρ, T_{e0} and n_{zc} are shown at the upper

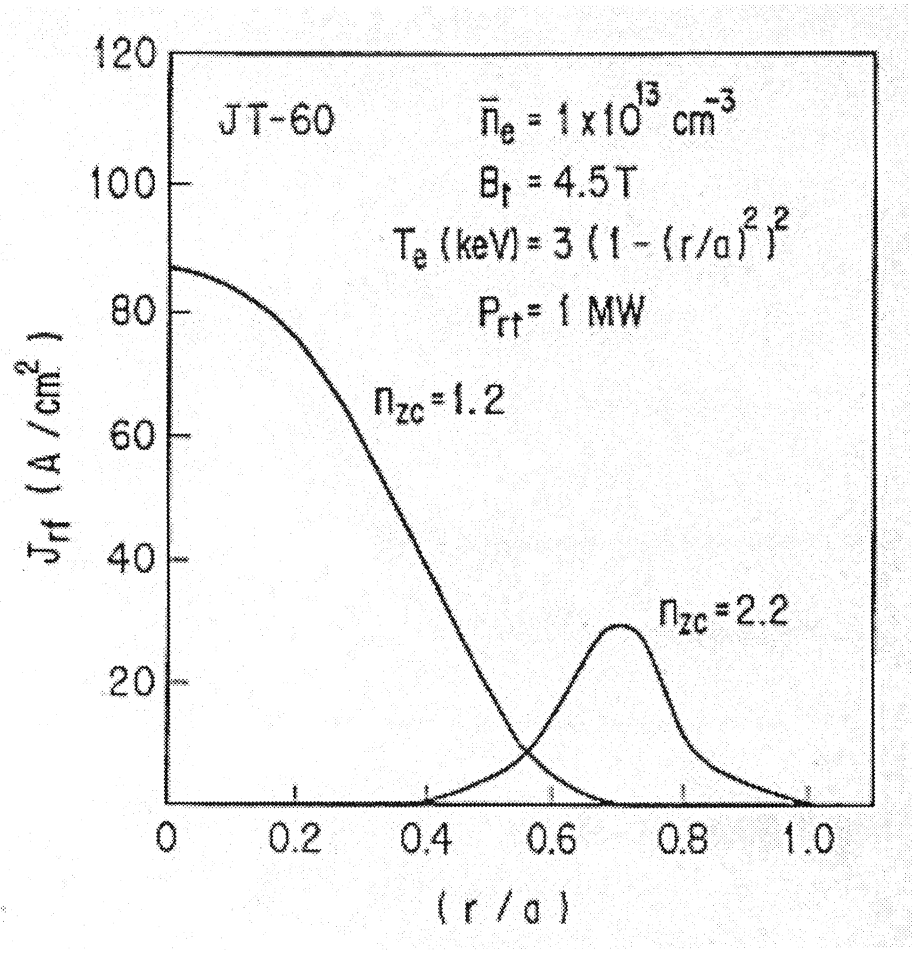

Fig. 7 Evaluated current profile for n_{zc}=1.2 and n_{zc}=2.2 in JT-60 parameter, where b=21.9, α=0.23, $\gamma_{\chi 1}$=1, γ_{c2}=4.24, P_{rf}= 1MW and ρ= 4 kW/cm^2.

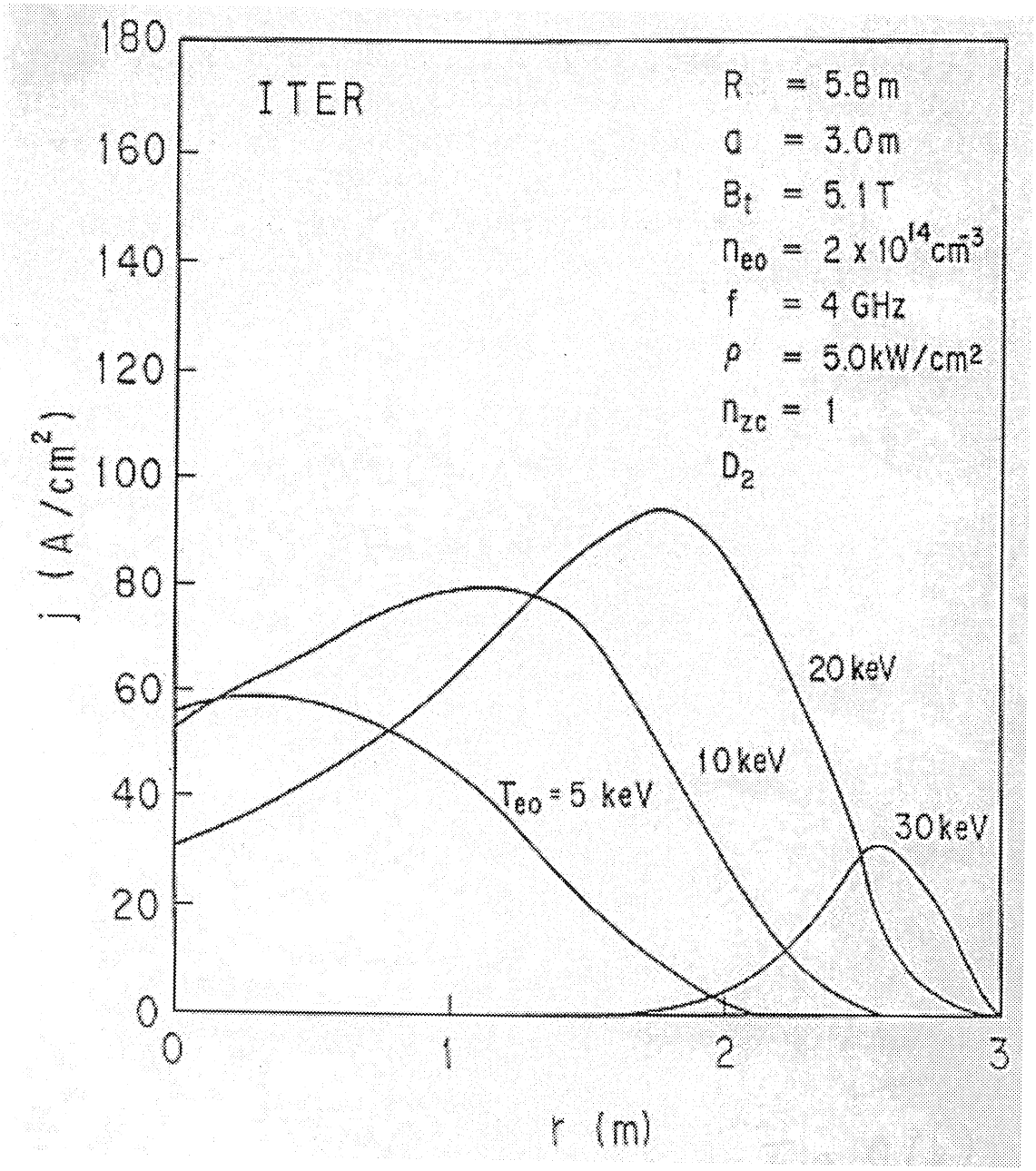

Fig. 8 Evaluated current profile putting T_{e0} as parameters in ITER parameters, where b=21.9, α=0.23, $\gamma_{\chi 1}$=1, γ_{c2}=4.24

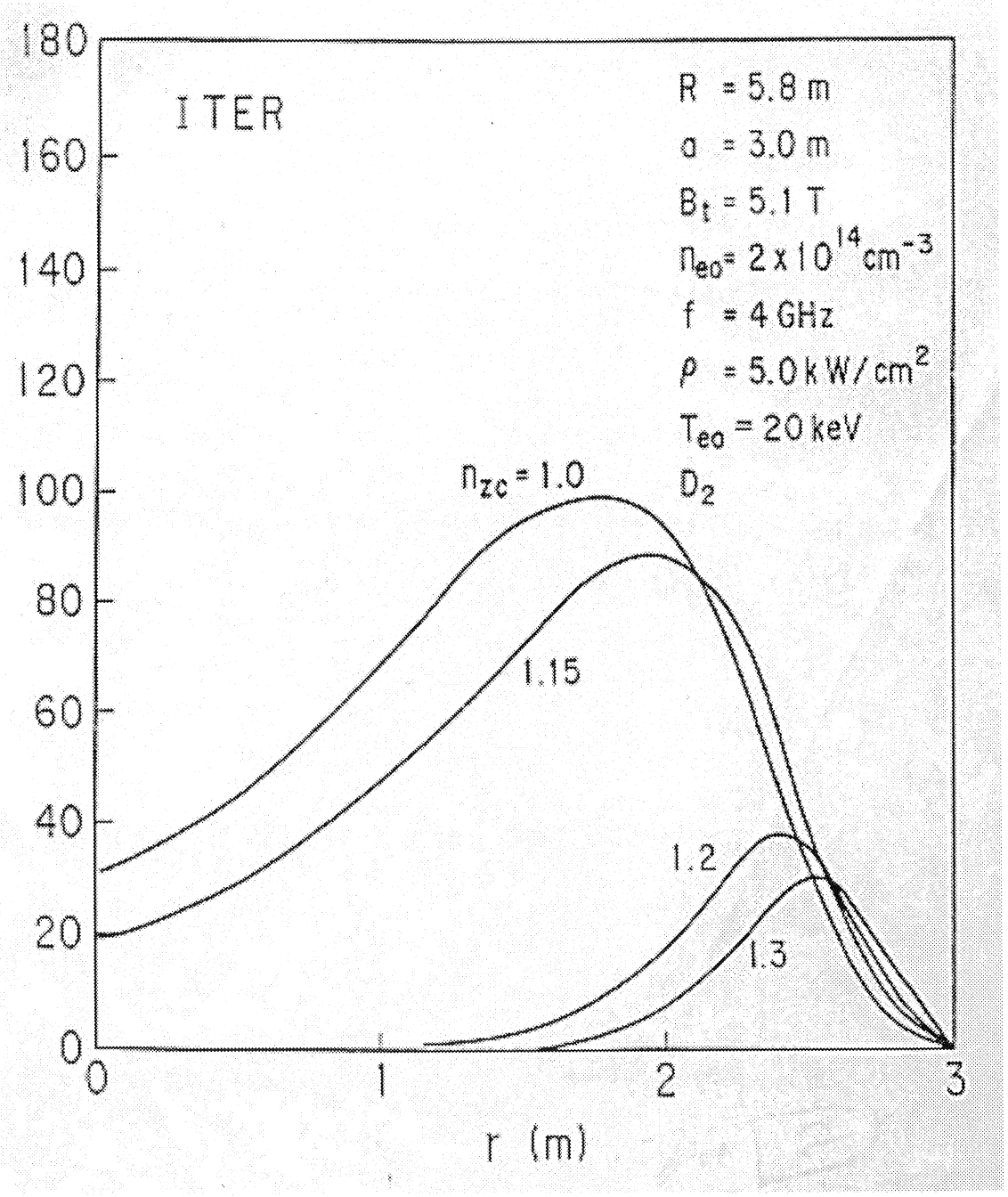

Fig. 9 Evaluated current profile putting n_{zc} in ITER parameter, where b=21.9, α=0.23, $\gamma_{\chi 1}$=1, γ_{c2}=4.42.

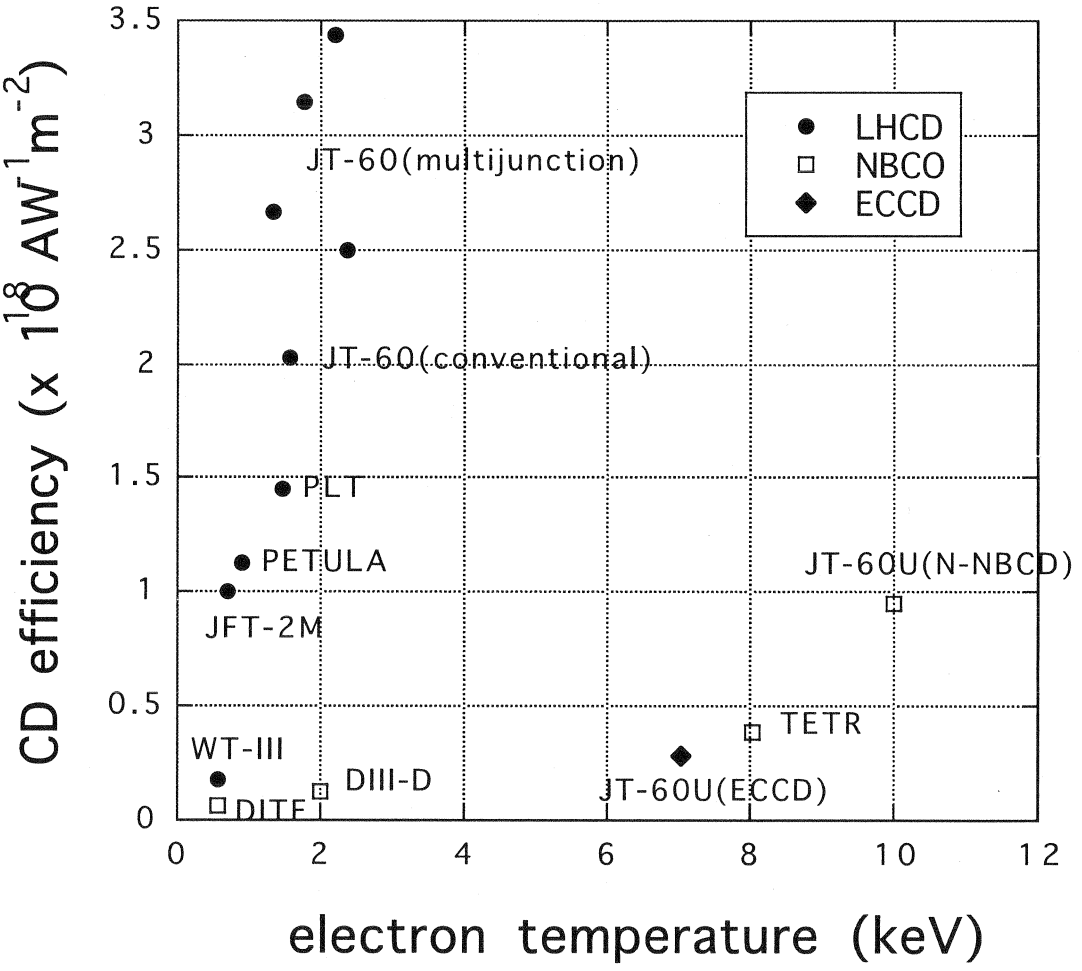

Fig. 10 Current drive efficiency η_{CD} against the electron temperature in various machines for LHCD, NBCD and ECCD. The notation of multijunction and conventional in JT-60 case means the launcher type of the LHCD and N-NBCD in JT-60U case means the NBCD by using negative ion beam.

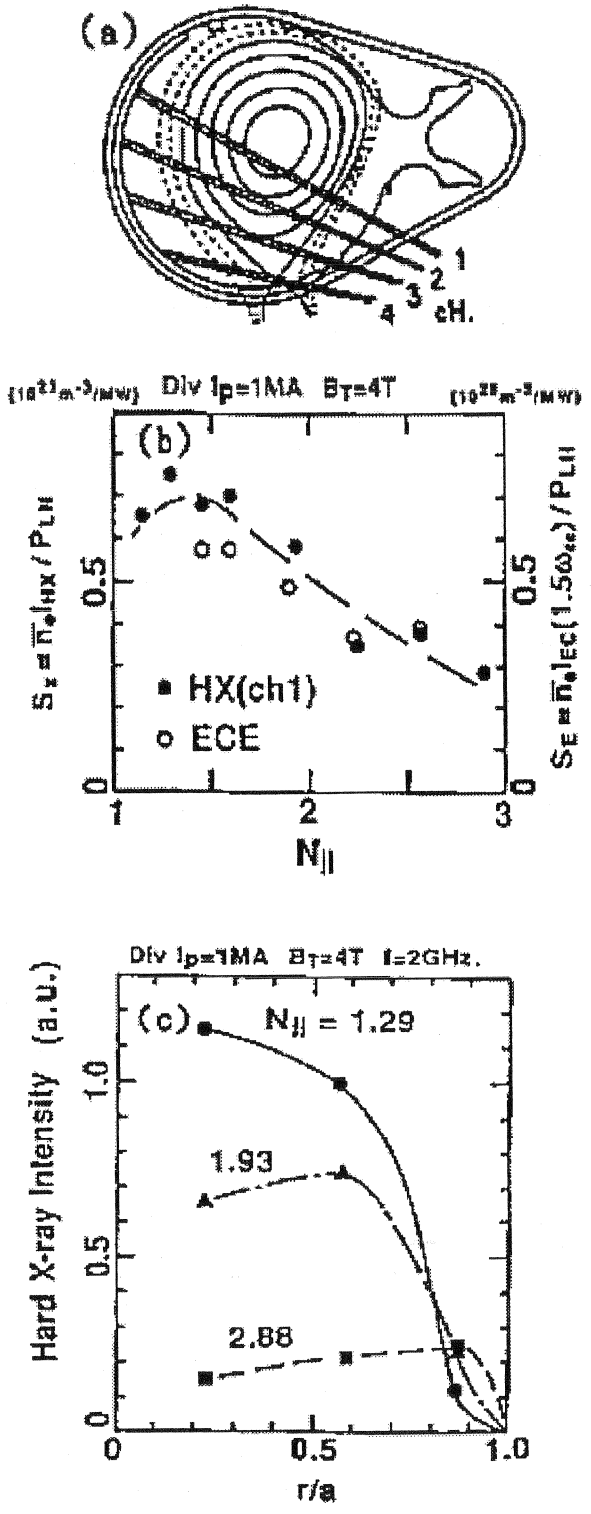

Fig. 11 Observed hard X ray signal in the radial direction which may correspond to the calculation in Fig. 4 and Fig. 7, respectively, where the experimental condition is $\bar{n}_e$= 1 x 10^{13} cm^{-3}, I_p= 1MA, f= 2 GHz and B_t= 4.0 T (a) the poloidal cross section equipping the hard X ray diagnostics (b) the intensity of the hard X ray signal against $N_{//}$ which corresponds to the evaluation of Fig. 4 (c) the radial profile for $N_{//}$ which corresponds to the evaluation of Fig.7.

国際単位系（SI）

表１．SI 基本単位

基本量	SI 基本単位	
	名称	記号
長さ	メートル	m
質量	キログラム	kg
時間	秒	s
電流	アンペア	A
熱力学温度	ケルビン	K
物質量	モル	mol
光度	カンデラ	cd

表２．基本単位を用いて表されるSI組立単位の例

組立量	SI 基本単位	
	名称	記号
面積	平方メートル	m^2
体積	立法メートル	m^3
速さ，速度	メートル毎秒	m/s
加速度	メートル毎秒毎秒	m/s^2
波数	毎メートル	m-1
密度（質量密度）	キログラム毎立法メートル	kg/m^3
質量体積（比体積）	立法メートル毎キログラム	m^3/kg
電流密度	アンペア毎平方メートル	A/m^2
磁界の強さ	アンペア毎メートル	A/m
（物質量の）濃度	モル毎立方メートル	mol/m^3
輝度	カンデラ毎平方メートル	cd/m^2
屈折率	（数の）1	1

表５．SI 接頭語

乗数	接頭語	記号	乗数	接頭語	記号
10^{24}	ヨタ	Y	10^{-1}	デシ	d
10^{21}	ゼタ	Z	10^{-2}	センチ	c
10^{18}	エクサ	E	10^{-3}	ミリ	m
10^{15}	ペタ	P	10^{-6}	マイクロ	μ
10^{12}	テラ	T	10^{-9}	ナノ	n
10^{9}	ギガ	G	10^{-12}	ピコ	p
10^{6}	メガ	M	10^{-15}	フェムト	f
10^{3}	キロ	k	10^{-18}	アト	a
10^{2}	ヘクト	h	10^{-21}	ゼプト	z
10^{1}	デカ	da	10^{-24}	ヨクト	y

表３．固有の名称とその独自の記号で表されるSI組立単位

組立量	SI 組立単位			
	名称	記号	他のSI単位による表し方	SI基本単位による表し方
平面角	ラジアン(a)	rad		$m \cdot m^{-1}=1$(b)
立体角	ステラジアン(a)	sr(c)		$m^2 \cdot m^{-2}=1$(b)
周波数	ヘルツ	Hz		s^{-1}
力	ニュートン	N		$m \cdot kg \cdot s^{-2}$
圧力，応力	パスカル	Pa	N/m^2	$m^{-1} \cdot kg \cdot s^{-2}$
エネルギー，仕事，熱量	ジュール	J	N・m	$m^2 \cdot kg \cdot s^{-2}$
工率，放射束	ワット	W	J/s	$m^2 \cdot kg \cdot s^{-3}$
電荷，電気量	クーロン	C		s・A
電位差（電圧），起電力	ボルト	V	W/A	$m^2 \cdot kg \cdot s^{-3} \cdot A^{-1}$
静電容量	ファラド	F	C/V	$m^{-2} \cdot kg^{-1} \cdot s^4 \cdot A^2$
電気抵抗	オーム	Ω	V/A	$m^2 \cdot kg \cdot s^{-3} \cdot A^{-2}$
コンダクタンス	ジーメンス	S	A/V	$m^{-2} \cdot kg^{-1} \cdot s^3 \cdot A^2$
磁束	ウエーバ	Wb	V・s	$m^2 \cdot kg \cdot s^{-2} \cdot A^{-1}$
磁束密度	テスラ	T	Wb/m^2	$kg \cdot s^{-2} \cdot A^{-1}$
インダクタンス	ヘンリー	H	Wb/A	$m^2 \cdot kg \cdot s^{-2} \cdot A^{-2}$
セルシウス温度	セルシウス度(d)	℃		K
光束	ルーメン	lm	cd・sr(c)	$m^2 \cdot m^{-2} \cdot cd=cd$
照度	ルクス	lx	lm/m^2	$m^2 \cdot m^{-4} \cdot cd=m^{-2} \cdot cd$
（放射性核種の）放射能	ベクレル	Bq		s^{-1}
吸収線量，質量エネルギー分与，カーマ	グレイ	Gy	J/kg	$m^2 \cdot s^{-2}$
線量当量，周辺線量当量，方向性線量当量，個人線量当量，組織線量当	シーベルト	Sv	J/kg	$m^2 \cdot s^{-2}$

(a)ラジアン及びステラジアンの使用は、同じ次元であっても異なった性質をもった量を区別するときの組立単位の表し方として利点がある。組立単位を形作るときのいくつかの用例は表４に示されている。
(b)実際には、使用する時には記号rad及びsrが用いられるが、習慣として組立単位としての記号“１”は明示されない。
(c)測光学では、ステラジアンの名称と記号srを単位の表し方の中にそのまま維持している。
(d)この単位は、例としてミリセルシウス度m℃のようにSI接頭語を伴って用いても良い。

表４．単位の中に固有の名称とその独自の記号を含むSI組立単位の例

組立量	SI 組立単位		
	名称	記号	SI 基本単位による表し方
粘度	パスカル秒	Pa・s	$m^{-1} \cdot kg \cdot s^{-1}$
力のモーメント	ニュートンメートル	N・m	$m^2 \cdot kg \cdot s^{-2}$
表面張力	ニュートン毎メートル	N/m	$kg \cdot s^{-2}$
角速度	ラジアン毎秒	rad/s	$m \cdot m^{-1} \cdot s^{-1}=s^{-1}$
角加速度	ラジアン毎平方秒	rad/s^2	$m \cdot m^{-1} \cdot s^{-2}=s^{-2}$
熱流密度，放射照度	ワット毎平方メートル	W/m^2	$kg \cdot s^{-3}$
熱容量，エントロピー	ジュール毎ケルビン	J/K	$m^2 \cdot kg \cdot s^{-2} \cdot K^{-1}$
質量熱容量（比熱容量），質量エントロピー	ジュール毎キログラム毎ケルビン	J/(kg・K)	$m^2 \cdot s^{-2} \cdot K^{-1}$
質量エネルギー（比エネルギー）	ジュール毎キログラム	J/kg	$m^2 \cdot s^{-2} \cdot K^{-1}$
熱伝導率	ワット毎メートル毎ケルビン	W/(m・K)	$m \cdot kg \cdot s^{-3} \cdot K^{-1}$
体積エネルギー	ジュール毎立方メートル	J/m^3	$m^{-1} \cdot kg \cdot s^{-2}$
電界の強さ	ボルト毎メートル	V/m	$m \cdot kg \cdot s^{-3} \cdot A^{-1}$
体積電荷	クーロン毎立方メートル	C/m^3	$m^{-3} \cdot s \cdot A$
電気変位	クーロン毎平方メートル	C/m^2	$m^{-2} \cdot s \cdot A$
誘電率	ファラド毎メートル	F/m	$m^{-3} \cdot kg^{-1} \cdot s^4 \cdot A^2$
透磁率	ヘンリー毎メートル	H/m	$m \cdot kg \cdot s^{-2} \cdot A^{-2}$
モルエネルギー	ジュール毎モル	J/mol	$m^2 \cdot kg \cdot s^{-2} \cdot mol^{-1}$
モルエントロピー，モル熱容量	ジュール毎モル毎ケルビン	J/(mol・K)	$m^2 \cdot kg \cdot s^{-2} \cdot K^{-1} \cdot mol^{-1}$
照射線量（X線及びγ線）	クーロン毎キログラム	C/kg	$kg^{-1} \cdot s \cdot A$
吸収線量率	グレイ毎秒	Gy/s	$m^2 \cdot s^{-3}$
放射強度	ワット毎ステラジアン	W/sr	$m^4 \cdot m^{-2} \cdot kg \cdot s^{-3}=m^2 \cdot kg \cdot s^{-3}$
放射輝度	ワット毎平方メートル毎ステラジアン	$W/(m^2 \cdot sr)$	$m^2 \cdot m^{-2} \cdot kg \cdot s^{-3}=kg \cdot s^{-3}$

表６．国際単位系と併用されるが国際単位系に属さない単位

名称	記号	SI 単位による値
分	min	1 min=60s
時	h	1h =60 min=3600 s
日	d	1 d=24 h=86400 s
度	°	$1° = (\pi/180)$ rad
分	’	$1’ = (1/60)° = (\pi/10800)$ rad
秒	”	$1” = (1/60)’ = (\pi/648000)$ rad
リットル	l、L	$1l=1\ dm^3=10^{-3}m^3$
トン	t	$1t=10^3$ kg
ネーパ	Np	1Np=1
ベル	B	1B=(1/2)ln10(Np)

表７．国際単位系と併用されこれに属さない単位で SI単位で表される数値が実験的に得られるもの

名称	記号	SI 単位であらわされる数値
電子ボルト	eV	$1eV=1.60217733(49) \times 10^{-19}J$
統一原子質量単位	u	$1u=1.6605402(10) \times 10^{-27}kg$
天文単位	ua	$1ua=1.49597870691(30) \times 10^{11}m$

表８．国際単位系に属さないが国際単位系と 併用されるその他の単位

名称	記号	SI 単位であらわされる数値
海里		1海里=1852m
ノット		1ノット=1海里毎時=(1852/3600)m/s
アール	a	$1a=1\ dam^2=10^2m^2$
ヘクタール	ha	$1ha=1\ hm^2=10^4m^2$
バール	bar	$1bar=0.1MPa=100kPa=1000hPa=10^5Pa$
オングストローム	Å	$1Å=0.1nm=10^{-10}m$
バーン	b	$1b=100fm^2=10^{-28}m^2$

表９．固有の名称を含むCGS組立単位

名称	記号	SI 単位であらわされる数値
エルグ	erg	$1\ erg=10^{-7}$ J
ダイン	dyn	$1\ dyn=10^{-5}N$
ポアズ	P	$1\ P=1\ dyn \cdot s/cm^2=0.1Pa \cdot s$
ストークス	St	$1\ St=1cm^2/s=10^{-4}m^2/s$
ガウス	G	$1\ G \triangleq 10^{-4}T$
エルステッド	Oe	$1\ Oe \triangleq (1000/4\pi)A/m$
マクスウェル	Mx	$1\ Mx \triangleq 10^{-8}Wb$
スチルブ	sb	$1\ sb=1cd/cm^2=10^4cd/m^2$
ホト	ph	$1\ ph=10^4lx$
ガル	Gal	$1\ Gal=1cm/s^2=10^{-2}m/s^2$

表10．国際単位に属さないその他の単位の例

名称	記号	SI 単位であらわされる数値
キュリー	Ci	$1\ Ci=3.7 \times 10^{10}Bq$
レントゲン	R	$1\ R = 2.58 \times 10^{-4}C/kg$
ラド	rad	$1\ rad=1cGy=10^{-2}Gy$
レム	rem	$1\ rem=1\ cSv=10^{-2}Sv$
X線単位		$1X\ unit=1.002 \times 10^{-4}nm$
ガンマ	γ	$1\ \gamma=1\ nT=10^{-9}T$
ジャンスキー	Jy	$1\ Jy=10^{-26}W \cdot m^{-2} \cdot Hz^{-1}$
フェルミ		$1\ fermi=1\ fm=10^{-15}m$
メートル系カラット		1 metric carat = 200 mg = 2×10^{-4}kg
トル	Torr	1 Torr = (101 325/760) Pa
標準大気圧	atm	1 atm = 101 325 Pa
カロリー	cal	
ミクロン	μ	$1\ \mu=1\mu m=10^{-6}m$

（第７版，1998年改訂）

この印刷物は再生紙を使用しています。